THE JOURNAL OF PHYSICAL CHEMISTRY Letters

pubs.acs.org/JPCL

Letter

Room-Temperature Defect Qubits in Ultrasmall Nanocrystals

Dávid Beke,* Jan Valenta, Gyula Károlyházy, Sándor Lenk, Zsolt Czigány, Bence Gábor Márkus, Katalin Kamarás, Ferenc Simon, and Adam Gali*

Cite This: *J. Phys. Chem. Lett.* 2020, 11, 1675−1681

Read Online

ACCESS | Metrics & More | Article Recommendations | Supporting Information

ABSTRACT: There is an urgent quest for room-temperature qubits in nanometer-sized, ultrasmall nanocrystals for quantum biosensing, hyperpolarization of biomolecules, and quantum information processing. Thus far, the preparation of such qubits at the nanoscale has remained futile. Here, we present a synthesis method that avoids any interaction of the solid with high-energy particles and uses self-propagated high-temperature synthesis with a subsequent electrochemical method, the no-photon exciton generation chemistry to produce room-temperature qubits in ultrasmall nanocrystals of sizes down to 3 nm with high yield. We first create the host silicon carbide (SiC) crystallites by high-temperature synthesis and then apply wet chemical etching, which results in ultrasmall SiC nanocrystals and facilitates the creation of thermally stable defect qubits in the material. We demonstrate room-temperature optically detected magnetic resonance signal of divacancy qubits with 3.5% contrast from these nanoparticles with emission wavelengths falling in the second biological window (1000−1380 nm). These results constitute the formation of nonperturbative bioagents for quantum sensing and efficient hyperpolarization.

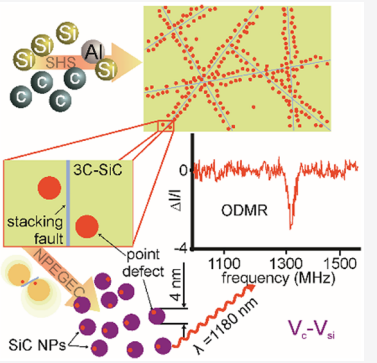

Solid state defect qubits are building blocks for quantum technology.[1] Room-temperature defect qubits[2−4] stand out with their great potential in biology and human diagnosis, by means of sensing at the nanoscale[5] and hyperpolarization of biomolecules.[6] The state of these defect qubits is read out by optical means which harness the spin-selective fluorescence of the defect qubits: the electron spin state can be manipulated by applying a resonant microwave field while monitoring changes in the fluorescence. This readout method is known as optically detected magnetic resonance (ODMR) spectroscopy.[2] Optical pumping of these ODMR defect qubits results in efficient electron spin polarization which can be transferred toward nuclear spins of the solid. This leads to a nuclear spin polarization around the defect qubits that can be several orders of magnitude larger than that in thermal equilibrium. This way the sensitivity of traditional magnetic resonance imaging (MRI)[6] and nuclear magnetic resonance (NMR)[7,8] techniques with defects in solids can be enhanced down to the few-molecule level.[9,10] In these applications, it is crucial to use small nanocrystals as nonperturbative agents[11] with qubits close to the surface for enhanced sensing and effective direct polarization of external nuclear spins. This requirement defines the diameter of the nanocrystals around 5 nm or below; we refer to these crystals as ultrasmall nanoparticles.[11,12]

Despite the fact that preparation of ultrasmall nanoparticles hosting stable qubits is appealing, the creation of such systems still remains a challenge. So far, ODMR signals from defect qubits have been either reported from 7.5 nm diamond nanocrystals, which were created by milling of larger crystals and subsequent electron irradiation,[13] or detected in some 5 nm particles separated from detonation nanodiamonds by ultracentrifugation.[14] The defect yield values in such systems are about 35% and 0.005−0.012 ppm, respectively. Later, the defect yield has been increased to a few fold[15] by electron irradiation and subsequent annealing at high temperature. Both methods create ultrasmall nanoparticles with a low quality of defects which was previously attributed to the presence of high strain and was manifested as a large splitting in the corresponding ODMR spectrum.[14] Furthermore, the 5 nm particle size could be a limit of formation of defect qubits in diamond by any preparation technique operating at elevated temperatures,[16] because of the competing and highly stable sp^2 carbon allotropes at sizes of a few nanometers.[17] Only a single study reported the photoluminescence (PL) signal of a qubit embedded in 1.5 nm diamonds that were found in special meteorites,[18] but this qubit only operates at cryogenic temperatures.[19] Silicon carbide (SiC), on the other hand, does not exhibit sp^2 allotropes which gives hope for the preparation of ultrasmall bioinert[20,21] SiC nanoparticles (NPs) with stable room-temperature qubits. However, the size of the smallest reported SiC NPs with the room-temperature ODMR signal of defect qubits, created by irradiation and milling, is 600 nm, and only PL signals were found in smaller particles with a size of 35 nm.[22]

Received: January 7, 2020
Accepted: February 10, 2020
Published: February 10, 2020

The lack of a suitable synthesis technique may be related, besides surface and crystal reconstruction, to the mechanism of qubit formation in ultrasmall nanoparticles. Indeed, all the known room-temperature defect qubits contain a vacancy,[2−4] a missing atom in the crystal structure, that has been predominantly created by implantation or irradiation techniques, by knocking out an atom from its lattice site,[4,9,22,23] to precisely control the defect location close to the surface, or to create vacancies uniformly in the bulk system before extensive milling, respectively. Both techniques lead to a cascade process forming unwanted multiple vacancies and other defects, that compromise the quality of the host crystal and affect the key operation parameters of the qubits.[24,25] Apart from detonation nanodiamonds,[26] qubits in small nanoparticles are often created by top-down methods: first, defect qubits are formed in larger crystallites by irradiation techniques and subsequent annealing, and then, they are milled or laser ablated into smaller crystals.[9,22,27] These procedures result in crystal quality dramatically affecting the performance of the qubits.[9,22]

Here, we report a novel technique for introducing room-temperature defect qubits into small nanoparticles that is similar to the principles of lithography and avoids any largely invasive material fabrication processes such as irradiation, implantation, and milling. We developed a chemical method that creates a high density of defects and a three-dimensional resist structure in the bulk material. The method also protects the defects and results in the formation of stable qubits during the electrochemical etching of this material while preparing the nanoparticles. By this method, we synthesized thermally stable qubits in 3−6 nm SiC nanoparticles with high yield. The ensemble of qubits exhibits room-temperature ODMR signals with 3.5% ODMR contrast, and near-infrared fluorescence, centered at 1180 nm at room temperature, most favorable for biological, medical, and telecommunication applications (Figure 1).

Defect Synthesis with Chemical Lithography. We used self-propagated high-temperature synthesis (SHS) starting from Si, C, and Al. A mixture of the precursor powders was placed into an induction furnace and heated up to about 1250 °C where Si and C react to create SiC. The heat generated by the reaction promotes fast conversion with high product yield. Aluminum (Al), on the other hand, reacts with SiC and removes silicon atoms from the crystal.[28,29] At the same time, Al promotes hexagonal crystal formation to the continuously growing SiC crystal.[30] This method creates cubic SiC powder with *in situ* generated point defects and a 3-dimensional network of stacking faults (SFs) that are two-dimensional hexagonal inclusions in the cubic matrix.[30]

Defect-Rich Nanoparticle Synthesis. SFs act as resists during the etching process known as no-photon exciton generation chemistry (NPEGEC),[30] that dissolves only cubic SiC producing ultrasmall SiC NPs and leaves intact the two-dimensional hexagonal inclusions[30] and the vacancies in the vicinity. We followed the transformations of defects by EPR and PL spectroscopy (see Figure 2). The as-synthesized SiC ceramic powder exhibits a strong EPR signal that corresponds to a silicon vacancy,[31] V_{Si} with $S = 3/2$ electron spin and characteristic double peaks due to the hyperfine interaction with ^{29}Si nuclear spins. The nonzero zero-field splitting value (27 MHz) indicates that these vacancies are close to the hexagonal SF layers that break the tetrahedral symmetry (Figure 2A). V_{Si} also has photoemission under excitation, and the PL emission is centered around 900−1000 nm that was

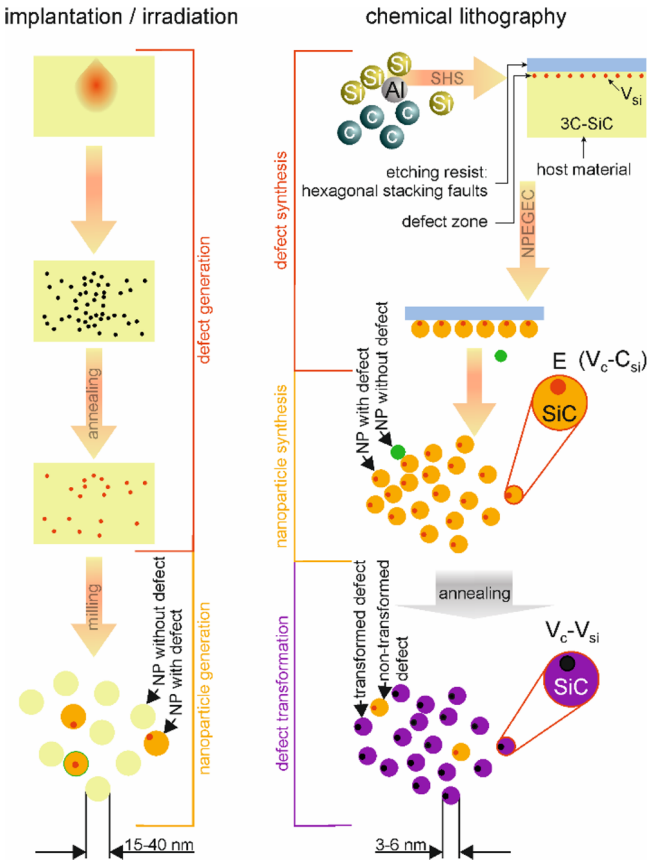

Figure 1. Schematic representation of the implantation or irradiation-based vacancy formation for preparation of nanoparticles with defect qubits versus chemical lithography techniques. Chemical lithography offers noninvasive nanoparticle synthesis of vacancy-related qubits with high yield. The benefit of chemical lithography is the formation of a three-dimensional resist network that protects the vacancies during nanoparticle synthesis. In the case of cubic SiC, Al additive during the synthesis leads both to stacking fault (SF) generation, i.e., a hexagonal SiC inclusion along a specific direction in the cubic lattice that is resistive against the no-photon exciton generation chemical etching (NPEGEC), and vacancy generation. Here, SFs act as resist, and NPEGEC synthesizes the nanoparticles. These nanoparticles contain an orange emitter (called the E center), originating from the carbon vacancy−antisite pair, V_C−C_{Si}. Annealing can transform E centers into divacancies, V_C−V_{Si} defects, that are near-infrared emitters with a room-temperature ODMR signal.

reported in hexagonal SiC crystals[22] (Figure 2B). This fact also implies that the preparation procedure creates these vacancies close to the hexagonal SF layers. NPEGEC etching creates a porous layer on the SiC surface that can be broken down to nanoparticles. The EPR and the PL spectra of the porous SiC and the nanoparticles indicate that V_{Si} in SiC is transformed into another type of vacancy after the NPEGEC process. NPEGEC was performed at around 180 °C (see the Supporting Information). Such temperature propagates diffusion of the vacancy at a few Ångströms scale, while the redox reactions change the surface creating oxygen-rich groups that shift the Fermi level. The process transforms the negatively charged V_{Si} into its more stable tautomer, the carbon antisite-vacancy defect,[32,33] namely, the E center,[34] which, in its double positively charged state,[34] shows a room-temperature maximum emission around 650 nm (Figure 2B), right in the first biological imaging window. The E center

https://dx.doi.org/10.1021/acs.jpclett.0c00052
J. Phys. Chem. Lett. 2020, 11, 1675−1681

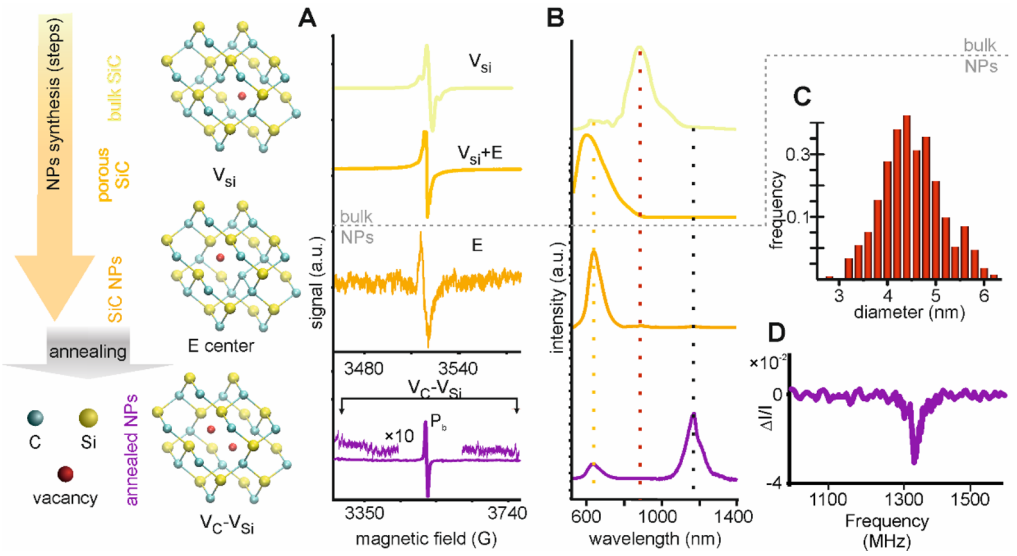

Figure 2. Monitoring the vacancy evaluation during the NPEGEC nanoparticle synthesis by the (A) *X*-band electron paramagnetic resonance spectrum and (B) photoluminescence spectrum. Bulk SiC contains silicon vacancies (V_{Si}) before chemical etching (yellow lines). NPEGEC creates porous SiC and transforms most of the V_{Si} into E centers. E centers show fluorescence predominantly in the first biological imaging window (centered at 650 nm with excitation wavelength: 550 nm) (light orange lines). These emission centers exist in 3−6 nm SiC NPs (dark orange lines, NPs in tetrahydrofuran). (C) Size distribution of the nanoparticles embedding E centers. A fraction of E centers was transformed into a near-infrared emitter, the divacancy, by annealing the NPs at 140 °C for 2 h: divacancies with $S = 1$ electron spin and broad emission in the 1050−1300 nm region were observed by (A) *X*-band EPR spectroscopy and (B) PL with excitation by a 785 nm laser, respectively (purple lines). The arrows in part A show the EPR transitions separated by zero-field splitting at 1327 MHz (474 gauss). The upper purple curve is a 10-fold magnification in intensity of the EPR spectrum where such EPR signals are more visible. Before annealing EPR shows only the signal of the single positively charged V_C−C_{Si} that we label by E center after its PL signal in its double positive charge state (dark orange line). After the annealing, a strong EPR signal with $g = 2.0043$ can also be observed (purple line in part A) that is associated with the Si dangling bond at the interface of SiC and amorphous SiO_2, i.e., a near-interface carbon vacancy (see the main text for additional details). (D) Room-temperature divacancy ODMR spectrum at zero magnetic field at 1327 MHz with PL excitation at 785 nm: ODMR contrast is 3.5%; the FWHM is 12 MHz.

fluorescence is detected in both porous SiC and 3−6 nm (Figure 2C) SiC NPs. The PL maximum is narrowed in the nanoparticles compared to that in porous SiC, indicating increasingly uniform surroundings.[22,34] It should be noted that E centers were characterized as single photon sources in porous SiC.[34] Only the doubly positively charged form of the vacancy is optically active, and because of that, E centers are sensitive to the environment when they are close to the surface, i.e., when the host material is an ultrasmall nanoparticle. The E center emission can be easily detected from dry nanoparticles or nanoparticles dispersed in tetrahydrofuran. In aqueous solution, E centers are active only in an alkaline environment, or when a proper surfactant is used (ultrasmall SiC nanoparticles can be dispersed in polar solvents without surfactants).

Transformation of the E Centers into the Paramagnetic Divacancy. We applied low-temperature annealing to transform the E centers in SiC NPs into an infrared emitter with $S = 1$ electron spin state, the divacancy (V_C−V_{Si}).[35] The drying process of SiC NPs causes the redistribution of the surface groups,[36−38] and decarboxylation[39,40] which generates near-surface vacancies.[39,40] A carbon vacancy, formed during annealing within a 3 neighbor distance to an E center, transforms to a divacancy.[35] The EPR signal of SiC NPs annealed at 140 °C can be seen in Figure 2A. A strong EPR signal with $g = 2.0043$ can be observed that is associated with the Si dangling bond at the interface of SiC and amorphous SiO_2[41,42] (P_b center), that can be viewed as a near-surface carbon vacancy. Indeed, carbon vacancies in SiC exhibit no PL but a strong EPR signal, while the divacancy shows the opposite behavior. V_C−V_{Si} defects in the nanoparticles have a random orientation, which leads to arbitrary orientations of the corresponding spin quantization axis. As the resonance frequency of this defect is highly dependent on the angle between the magnetic field and the spin quantization axis,[43] the EPR spectrum of V_C−V_{Si} in SiC powder becomes very broad. However, sharp features arise at certain orientations,[44] corresponding to the divacancy EPR signal[45] in the SiC NPs (Figure 2A). The V_C−V_{Si} defect emits light at around 1180 nm, at the center of the second biological imaging window, where deep tissue imaging is possible because of the reduced light absorption and scattering (Figure 2B). Besides the PL spectrum, direct identification of these centers is provided by the detected ODMR signal which shows a clear electron spin resonance at 1327 MHz, in excellent agreement with the reported value in the Ky5 electron paramagnetic resonance (EPR) center[43] and ODMR center[4,45] associated with a divacancy in cubic SiC (Figure 2D). The measured full width at half maximum (FWHM) of 12 MHz at room temperature agrees well with the fwhm of ensembles of divacancies with favorable qubit properties,[3,4] and the observed 3.5% ODMR contrast is also consistent with the latest studies on divacancies in cubic SiC.[46] We emphasize that the detected ODMR signals do not show any evidence of splitting due to external perturbation in the few nanometers SiC nanoparticles. We note that a neutral divacancy does not require additional dopants like the negatively charged NV center in diamond. Dopants may create strain or stray electric fields upon illumination causing large splitting in the corresponding ODMR spectra that occurs for NV centers in nanodiamonds.

https://dx.doi.org/10.1021/acs.jpclett.0c00052
J. Phys. Chem. Lett. 2020, 11, 1675−1681

Determination of the Defect Yield in Nanoparticles. We determined the defect yield of the vacancy with the photoluminescence of the E center by using single dot PL spectroscopy[47] on drop-cast samples and PL spectroscopy in aqueous solutions. The first method was applied to 217 individual nanoparticles, whereas the second method samples millions of nanoparticles. Single dot spectroscopy measures the emission spectra of individual NPs (Figure 3A), and the yield can be determined by the frequency ratio between particles that have different colors (Figure 3B) (i.e., the nanoparticles which contain the E centers have emission centered around 600−700 nm, and defect-free particles emit in the range 450−550 nm). In aqueous solution, the E center is dark at neutral pH because the surface charge alters the distribution of photoexcited carriers, but it becomes visible in alkaline solution. As a result, all particles emit around 530 nm at neutral pH, but nanoparticles containing the E center have a maximum emission around 620 nm in alkaline solution, while the emission of the defect-free particles is unaffected. Consequently, the band-edge PL intensity at 530 nm decreases proportionally to the particles hosting the E centers (Figure 3C). Single dot spectroscopy of dried samples and PL spectroscopy in aqueous solution give 57% and 60% yield, respectively.

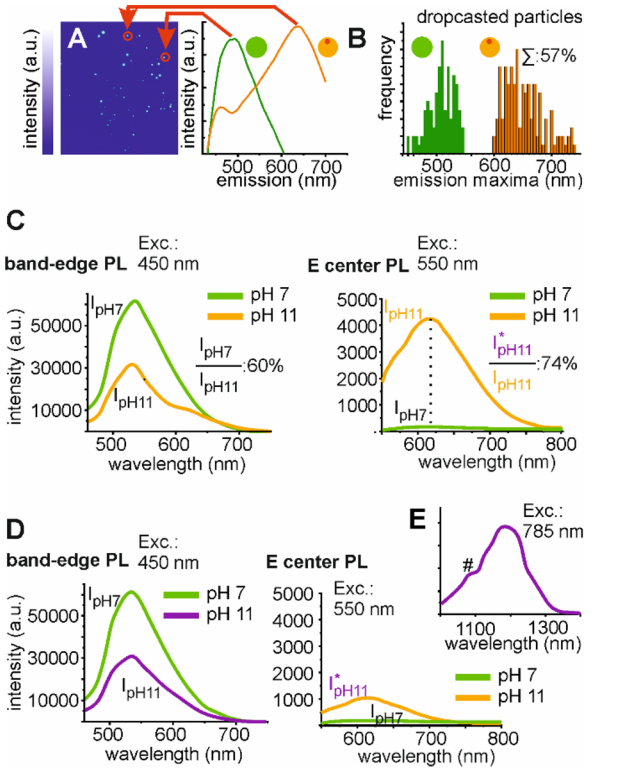

Figure 3. Determination of the defect yield. (A) Single dot spectroscopy measures the spectrum of individual NPs (excitation wavelength: 405 nm). NPs with E centers emit above 600 nm, while defect-free nanoparticles emit below 550 nm. (B) From the ratio between the two emitters, the defect yield can be estimated. (C) The E center is dark in aqueous solution at pH 7, and all the nanoparticles show band-edge luminescence (excitation wavelength: 450 nm). In alkaline solution by converting pH 7 to pH 11, the E center becomes active, which results in a new emission at around 620 nm and a decrease of the band-edge luminescence. The intensity ratio of the band-edge luminescence between the two states gives an estimate of the defect yield. Single dot spectroscopy on a drop-cast sample and luminescence spectroscopy in solution give almost the same result. (D) Annealing of NPs transforms a fraction of E centers into divacancies which results in a decrease of the E center emission (excitation wavelength: 550 nm). The intensity ratio of the E center emission before and after the annealing was used to estimate the conversion yield. (E) Infrared emission of the divacancies in the middle of the second biological window in aqueous solution (excitation wavelength: 785 nm). The octothorp here indicates the water Raman peak under 785 nm excitation. Green lines represent band-edge emission from drop-cast samples in part A or from aqueous solutions at pH 7 in parts C and D, where only the band-edge emission can be seen. Orange lines in part B are the emission of the E center from drop-cast samples, or the emission of the alkaline solution before annealing in part C, in which defect emissions are activated. The spectra of the annealed samples are colored purple in parts D and E.

From PL measurements, it is possible to determine the conversion of the E centers into divacancies, too, by measuring the intensity ratio of the E center emission between the nonannealed and annealed samples. The band-to-band recombination shows the same intensity before and after annealing and the same decrease in alkaline solution (Figure 3D) as divacancies are active only in alkaline solution, too (Figure 3E). The PL intensity of the E center in aqueous solution after the annealing was reduced to 26% of that before annealing (Figure 3D). One can estimate from this observation that the conversion efficiency is around 74%. From the change in the intensity of EPR signals we estimate a similar conversion efficiency (see the Supporting Information).

In conclusion, the advance in the field of detectors for the wavelength region of the second biological window and lock-in techniques makes our silicon carbide divacancy nanoparticles with strain-free ODMR signals very attractive for various quantum-technology-related applications. Our findings pave the way toward quantum biosensing, and efficient hyperpolarization of MRI contrast agents and biomolecules. As the yield of suitable nanoparticles is close to 40% with our present method, this can be directly applied in biochemistry and biolabeling without introducing postselection methods. The divacancy is embedded in ultrasmall cubic silicon carbide nanoparticles; the host nanoparticles were successfully tested in toxicity assays.[20,21] The efficient polarization of the divacancies' electron spin by optical pumping and spin polarization transfer toward proximate and distant nuclear spins at low constant magnetic fields has been already demonstrated.[48,49] All of these facts make these nanoparticles appealing as MRI contrast agents by utilizing the recent new methods of spin polarization transfer that may overcome the bottleneck of the ∼1.3 GHz zero-field-splitting pointing at arbitrary angles with respect to the direction of the external magnetic field in the powder samples.[50,51] The estimated distance between the divacancy and the surface is about 1 nm which makes the direct polarization of external nuclear spins very likely; thus, the idea of a polarizer device[52] can be directly applied for our nanoparticles. We further note that the emission wavelength with the center at the second biological window implies the deepest penetration depth by light among the known fluorophores in biological studies. In particular, the ODMR transition of divacancies is sensitive to the presence of external currents or electric fields,[53] e.g., induced by neuron cell activities, and thus can be an ultimate fluorescent biomarker for brain science.

https://dx.doi.org/10.1021/acs.jpclett.0c00052
J. Phys. Chem. Lett. 2020, 11, 1675−1681

■ ASSOCIATED CONTENT

Supporting Information

The Supporting Information is available free of charge at https://pubs.acs.org/doi/10.1021/acs.jpclett.0c00052.

Detailed materials and methods and detailed descriptions of analytical techniques such as particle size analysis, ESR, UV−vis absorption and visible photoluminescence spectroscopy, single-dot spectroscopy, near-infrared PL, and ODMR measurements (PDF)

■ AUTHOR INFORMATION

Corresponding Authors

Dávid Beke − *Institute for Solid State Physics and Optics, Wigner Research Centre for Physics, Budapest H-1525, Hungary; Department of Atomic Physics, Budapest University of Technology and Economics, Budapest H-1111, Hungary;* orcid.org/0000-0001-6046-8164; Email: beke.david@wigner.mta.hu

Adam Gali − *Institute for Solid State Physics and Optics, Wigner Research Centre for Physics, Budapest H-1525, Hungary; Department of Atomic Physics, Budapest University of Technology and Economics, Budapest H-1111, Hungary;* orcid.org/0000-0002-3339-5470; Email: gali.adam@wigner.mta.hu

Authors

Jan Valenta − *Faculty of Mathematics and Physics, Department of Chemical Physics & Optics, Charles University, Prague 12116, Czechia*

Gyula Károlyházy − *Institute for Solid State Physics and Optics, Wigner Research Centre for Physics, Budapest H-1525, Hungary*

Sándor Lenk − *Department of Atomic Physics, Budapest University of Technology and Economics, Budapest H-1111, Hungary*

Zsolt Czigány − *Institute for Technical Physics and Materials Science, Centre for Energy Research, Budapest H-1121, Hungary*

Bence Gábor Márkus − *Department of Physics, Budapest University of Technology and Economics and MTA-BME Lendület Spintronics Research Group (PROSPIN), Budapest H-1111, Hungary*

Katalin Kamarás − *Institute for Solid State Physics and Optics, Wigner Research Centre for Physics, Budapest H-1525, Hungary;* orcid.org/0000-0002-0390-3331

Ferenc Simon − *Department of Physics, Budapest University of Technology and Economics and MTA-BME Lendület Spintronics Research Group (PROSPIN), Budapest H-1111, Hungary*

Complete contact information is available at: https://pubs.acs.org/10.1021/acs.jpclett.0c00052

Author Contributions

D.B. contributed to the sample preparation, analysis of the EPR spectra, TEM, AFM, DLS results, PL, single dot PL, and ODMR measurements and analysis. J.V. carried out the single dot measurements and supervised the analysis. Gy.K. contributed to the sample preparation, PL, and EPR measurements. S.L. carried out the atomic force microscopy measurements. Zs.Cz. carried out high-resolution transmission electron microscopy measurements. B.G.M. recorded the EPR spectra under F.S.'s supervision. K.K. contributed to the near-infrared PL measurements. A.G. conceived the research project and wrote the manuscript with D.B. All authors commented on the manuscript.

Notes

The authors declare the following competing financial interest(s): D.B. and A.G. are inventors on patent application P1900269 related to this work.

Data and materials availability: All data are available in the main text or the Supporting Information. Additional data related to this paper may be requested from the authors.

■ ACKNOWLEDGMENTS

Support from the BME-Nanotechnology FIKP grant of EMMI (BME FIKP-NAT), the National Research Development and Innovation Office of Hungary grants NVKP_16-1-2016-0043, KK119442, NN127069, and NN127902 (EU QuantERA project Nanospin), as well as within the Quantum Technology National Excellence Program (Project Contract 2017-1.2.1-NKP-2017-00001) is acknowledged. D.B. acknowledges the following support: NTP-NFTÖ-18-B-0243 national talent program, the János Bolyai Scholarship of the Hungarian Academy of Sciences, and UNKP-19 New National Excellence program. J.V. is grateful for the support of the Charles University research center UNCE/SCI/010.

■ REFERENCES

(1) Eckstein, J. N.; Levy, J. Materials Issues for Quantum Computation. *MRS Bull.* **2013**, *38*, 783−789.

(2) Gruber, A.; Drabenstedt, A.; Tietz, C.; Fleury, L.; Wrachtrup, J.; Von Borczyskowski, C.; Gruber, A.; Dra, A.; Tietz, C.; Fleury, L.; et al. Scanning Confocal Optical Microscopy and Magnetic Resonance on Single Defect Centers. *Science* **1997**, *276*, 2012−2014.

(3) Koehl, W. F.; Buckley, B. B.; Heremans, F. J.; Calusine, G.; Awschalom, D. D. Room Temperature Coherent Control of Defect Spin Qubits in Silicon Carbide. *Nature* **2011**, *479*, 84−87.

(4) Falk, A. L.; Buckley, B. B.; Calusine, G.; Koehl, W. F.; Dobrovitski, V. V.; Politi, A.; Zorman, C. A.; Feng, P. X.-L.; Awschalom, D. D. Polytype Control of Spin Qubits in Silicon Carbide. *Nat. Commun.* **2013**, *4*, 1819.

(5) Kucsko, G.; Maurer, P. C.; Yao, N. Y.; Kubo, M.; Noh, H. J.; Lo, P. K.; Park, H.; Lukin, M. D. Nanometre-Scale Thermometry in a Living Cell. *Nature* **2013**, *500*, 54−58.

(6) Fernández-Acebal, P.; Rosolio, O.; Scheuer, J.; Müller, C.; Müller, S.; Schmitt, S.; McGuinness, L. P.; Schwarz, I.; Chen, Q.; Retzker, A.; et al. Toward Hyperpolarization of Oil Molecules via Single Nitrogen Vacancy Centers in Diamond. *Nano Lett.* **2018**, *18*, 1882−1887.

(7) Staudacher, T.; Shi, F.; Pezzagna, S.; Meijer, J.; Du, J.; Meriles, C. A.; Reinhard, F.; Wrachtrup, J. Nuclear Magnetic Resonance Spectroscopy on a (5-Nanometer) 3 Sample Volume. *Science* **2013**, *339*, 561−563.

(8) Schmitt, S.; Gefen, T.; Stürner, F. M.; Unden, T.; Wolff, G.; Müller, C.; Scheuer, J.; Naydenov, B.; Markham, M.; Pezzagna, S.; et al. Submillihertz Magnetic Spectroscopy Performed with a Nanoscale Quantum Sensor. *Science* **2017**, *356*, 832−837.

(9) Wu, Y.; Jelezko, F.; Plenio, M. B.; Weil, T. Diamond Quantum Devices in Biology. *Angew. Chem., Int. Ed.* **2016**, *55*, 6586−6598.

(10) Bucher, D. B.; Glenn, D. R.; Park, H.; Lukin, M. D.; Walsworth, R. L. Hyperpolarization-Enhanced NMR Spectroscopy with Femtomole Sensitivity Using Quantum Defects in Diamond. 2018, arXiv:1810.02408 No. 1. arXiv preprint. https://arxiv.org/abs/1810.02408.

(11) Choi, H. S.; Liu, W.; Misra, P.; Tanaka, E.; Zimmer, J. P.; Itty Ipe, B.; Bawendi, M. G.; Frangioni, J. V. Renal Clearance of Quantum Dots. *Nat. Biotechnol.* **2007**, *25*, 1165−1170.

(12) Wrachtrup, J.; Jelezko, F.; Grotz, B.; McGuinness, L. Nitrogen-Vacancy Centers Close to Surfaces. *MRS Bull.* **2013**, *38*, 149−154.
(13) Tisler, J.; Balasubramanian, G.; Naydenov, B.; Kolesov, R.; Grotz, B.; Reuter, R.; Boudou, J.-P.; Curmi, P. A.; Sennour, M.; Thorel, A.; et al. Fluorescence and Spin Properties of Defects in Single Digit Nanodiamonds. *ACS Nano* **2009**, *3*, 1959−1965.
(14) Bradac, C.; Gaebel, T.; Naidoo, N.; Sellars, M. J.; Twamley, J.; Brown, L. J.; Barnard, A. S.; Plakhotnik, T.; Zvyagin, A. V.; Rabeau, J. R. Observation and Control of Blinking Nitrogen-Vacancy Centres in Discrete Nanodiamonds. *Nat. Nanotechnol.* **2010**, *5*, 345−349.
(15) Terada, D.; Segawa, T. F.; Shames, A. I.; Onoda, S.; Ohshima, T.; Ōsawa, E.; Igarashi, R.; Shirakawa, M. Monodisperse Five-Nanometer-Sized Detonation Nanodiamonds Enriched in Nitrogen-Vacancy Centers. *ACS Nano* **2019**, *13*, 6461−6468.
(16) Barnard, A. S. Theory and Modeling of Nanocarbon Phase Stability. *Diamond Relat. Mater.* **2006**, *15*, 285−291.
(17) De Vita, A.; Galli, G.; Canning, A.; Car, R. A Microscopic Model for Surface-Induced Diamond-to-Graphite Transitions. *Nature* **1996**, *379*, 523−526.
(18) Vlasov, I. I.; Shiryaev, A. A.; Rendler, T.; Steinert, S.; Lee, S.-Y.; Antonov, D.; Vörös, M.; Jelezko, F.; Fisenko, A. V.; Semjonova, L. F.; et al. Molecular-Sized Fluorescent Nanodiamonds. *Nat. Nanotechnol.* **2014**, *9*, 54−58.
(19) Hepp, C.; Müller, T.; Waselowski, V.; Becker, J. N.; Pingault, B.; Sternschulte, H.; Steinmüller-Nethl, D.; Gali, A.; Maze, J. R.; Atatüre, M.; et al. Electronic Structure of the Silicon Vacancy Color Center in Diamond. *Phys. Rev. Lett.* **2014**, *112*, No. 036405.
(20) Saddow, S. E. *Silicon Carbide Biotechnology*, 2nd ed.; Elsevier Inc, 2016.
(21) Beke, D.; Szekrényes, Z.; Pálfi, D.; Róna, G.; Balogh, I.; Maák, P. A.; Katona, G.; Czigány, Z.; Kamarás, K.; Rózsa, B.; et al. Silicon Carbide Quantum Dots for Bioimaging. *J. Mater. Res.* **2013**, *28*, 205−209.
(22) Muzha, A.; Fuchs, F.; Tarakina, N. V.; Simin, D.; Trupke, M.; Soltamov, V. A.; Mokhov, E. N.; Baranov, P. G.; Dyakonov, V.; Krueger, A.; et al. Room-Temperature near-Infrared Silicon Carbide Nanocrystalline Emitters Based on Optically Aligned Spin Defects. *Appl. Phys. Lett.* **2014**, *105*, 243112.
(23) Havlik, J.; Petrakova, V.; Kucka, J.; Raabova, H.; Panek, D.; Stepan, V.; Zlamalova Cilova, Z.; Reineck, P.; Stursa, J.; Kucera, J.; et al. Extremely Rapid Isotropic Irradiation of Nanoparticles with Ions Generated in Situ by a Nuclear Reaction. *Nat. Commun.* **2018**, *9*, 4467.
(24) Deák, P.; Aradi, B.; Kaviani, M.; Frauenheim, T.; Gali, A. Formation of NV Centers in Diamond: A Theoretical Study Based on Calculated Transitions and Migration of Nitrogen and Vacancy Related Defects. *Phys. Rev. B: Condens. Matter Mater. Phys.* **2014**, *89*, No. 075203.
(25) Fávaro de Oliveira, F.; Antonov, D.; Wang, Y.; Neumann, P.; Momenzadeh, S. A.; Häußermann, T.; Pasquarelli, A.; Denisenko, A.; Wrachtrup, J. Tailoring Spin Defects in Diamond by Lattice Charging. *Nat. Commun.* **2017**, *8*, 15409.
(26) Froumin, N.; Prabhakar, N.; Giordani, S.; Reineck, P.; Torelli, M. D.; Vlasov, I.; Rosenholm, J. M.; Gibson, B.; Panich, A. M.; Nunn, N.; et al. Fluorescent Single-Digit Detonation Nanodiamond for Biomedical Applications. *Methods Appl. Fluoresc.* **2018**, *6*, No. 035010.
(27) Castelletto, S.; Almutairi, A. F. M.; Thalassinos, G.; Lohrmann, A.; Buividas, R.; Lau, D. W. M.; Reineck, P.; Juodkazis, S.; Ohshima, T.; Gibson, B. C.; et al. Fluorescent Color Centers in Laser Ablated 4H-SiC Nanoparticles. *Opt. Lett.* **2017**, *42*, 1297.
(28) Viala, J. C.; Bosselet, F.; Laurent, V.; Lepetitcorps, Y. Mechanism and Kinetics of the Chemical Interaction between Liquid Aluminium and Silicon-Carbide Single Crystals. *J. Mater. Sci.* **1993**, *28*, 5301−5312.
(29) Du, H.; Yang, Z.; Libera, M.; Jacobson, D. C.; Wang, Y. C.; Davis, R. F. Chemistry and Structure of Beta Silicon Carbide Implanted with High-Dose Aluminum. *J. Am. Ceram. Soc.* **1993**, *76*, 330−335.
(30) Beke, D.; Károlyházy, G.; Czigány, Z.; Bortel, G.; Kamarás, K.; Gali, A. Harnessing No-Photon Exciton Generation Chemistry to Engineer Semiconductor Nanostructures. *Sci. Rep.* **2017**, *7*, 10599.
(31) Itoh, H.; Kawasuso, A.; Ohshima, T.; Yoshikawa, M.; Nashiyama, I.; Tanigawa, S.; Misawa, S.; Okumura, H.; Yoshida, S. Intrinsic Defects in Cubic Silicon Carbide. *Phys. Stat. Sol. a* **1997**, *162*, 173−198.
(32) Bockstedte, M.; Mattausch, A.; Pankratov, O. Ab Initio Study of the Migration of Intrinsic Defects in 3 C − SiC. *Phys. Rev. B: Condens. Matter Mater. Phys.* **2003**, *68*, 205201.
(33) Rauls, E.; Lingner, T.; Hajnal, Z.; Greulich-Weber, S.; Frauenheim, T.; Spaeth, J.-M. Metastability of the Neutral Silicon Vacancy in 4H-SiC. *Phys. Status Solidi B* **2000**, *217*, R1−R3.
(34) Castelletto, S.; Johnson, B. C.; Zachreson, C.; Beke, D.; Balogh, I.; Ohshima, T.; Aharonovich, I.; Gali, A. Room Temperature Quantum Emission from Cubic Silicon Carbide Nanoparticles. *ACS Nano* **2014**, *8*, 7938−7947.
(35) Carlsson, P.; Son, N. T.; Gali, A.; Isoya, J.; Morishita, N.; Ohshima, T.; Magnusson, B.; Janzén, E. EPR and Ab Initio Calculation Study on the EI4 Center in 4*H*- and 6*H*-SiC. *Phys. Rev. B: Condens. Matter Mater. Phys.* **2010**, *82*, 235203.
(36) Szekrényes, Z.; Somogyi, B.; Beke, D.; Károlyházy, G.; Balogh, I.; Kamarás, K.; Gali, A. Chemical Transformation of Carboxyl Groups on the Surface of Silicon Carbide Quantum Dots. *J. Phys. Chem. C* **2014**, *118*, 19995−20001.
(37) Soukiassian, P.; Amy, F. Silicon Carbide Surface Oxidation and SiO_2/SiC Interface Formation Investigated by Soft X-ray Synchrotron Radiation. *J. Electron Spectrosc. Relat. Phenom.* **2005**, *144*−*147*, 783−788.
(38) Powers, J. M.; Somorjai, G. A. The Surface Oxidation of Alpha-Silicon Carbide by O_2 from 300 to 1373 K. *Surf. Sci.* **1991**, *244*, 39−50.
(39) Brown, B. R.; Phil, M. A. The Mechanism of Thermal Decarboxylation. *Q. Rev., Chem. Soc.* **1951**, *5*, 131−146.
(40) Englert, J. M.; Dotzer, C.; Yang, G.; Schmid, M.; Papp, C.; Gottfried, J. M.; Steinrück, H. P.; Spiecker, E.; Hauke, F.; Hirsch, A. Covalent Bulk Functionalization of Graphene. *Nat. Chem.* **2011**, *3*, 279−286.
(41) von Bardeleben, H. J.; Cantin, J. L.; Ke, L.; Shishkin, Y.; Devaty, R. P.; Choyke, W. J. Interface Defects in N-Type 3C-SiC/SiO_2: An EPR Study of Oxidized Porous Silicon Carbide Single Crystals. *Mater. Sci. Forum* **2005**, *483*−*485*, 273−276.
(42) Umeda, T.; Esaki, K.; Kosugi, R.; Fukuda, K.; Morishita, N.; Ohshima, T.; Isoya, J. Electrically Detected ESR Study of Interface Defects in 4H-SiC Metal-Oxide-Semiconductor Field Effect Transistor. *Mater. Sci. Forum* **2011**, *679*−*680*, 370−373.
(43) Bratus', V. Y.; Melnik, R. S.; Okulov, S. M.; Rodionov, V. N.; Shanina, B. D.; Smoliy, M. I. A New Spin One Defect in Cubic SiC. *Phys. B* **2009**, *404*, 4739−4741.
(44) de Biasi, R. S.; Mendonca, J. A. M. Powder ESR Spectra of Paramagnetic Impurities in Axial Symmetry Sites. *J. Magn. Reson.* **1983**, *53*, 462−472.
(45) Son, N. T.; Sörman, E.; Chen, W. M.; Hallin, C.; Kordina, O.; Monemar, B.; Janzén, E.; Lindström, J. L. Optically Detected Magnetic Resonance Studies of Defects in Electron-Irradiated 3C SiC Layers. *Phys. Rev. B: Condens. Matter Mater. Phys.* **1997**, *55*, 2863−2866.
(46) Wolfowicz, G.; Anderson, C. P.; Yeats, A. L.; Whiteley, S. J.; Niklas, J.; Poluektov, O. G.; Heremans, F. J.; Awschalom, D. D. Optical Charge State Control of Spin Defects in 4H-SiC. *Nat. Commun.* **2017**, *8*, 1876.
(47) Beke, D.; Fučíková, A.; Jánosi, T. Z.; Károlyházy, G.; Somogyi, B.; Lenk, S.; Krafcsik, O.; Czigány, Z.; Erostyák, J.; Kamarás, K.; et al. Direct Observation of Transition from Solid-State to Molecular-Like Optical Properties in Ultrasmall Silicon Carbide Nanoparticles. *J. Phys. Chem. C* **2018**, *122*, 26713−26721.
(48) Falk, A. L.; Klimov, P. V.; Ivády, V.; Szász, K.; Christle, D. J.; Koehl, W. F.; Gali, Á.; Awschalom, D. D. Optical Polarization of Nuclear Spins in Silicon Carbide. *Phys. Rev. Lett.* **2015**, *114*, 247603.

https://dx.doi.org/10.1021/acs.jpclett.0c00052
J. Phys. Chem. Lett. 2020, 11, 1675−1681

(49) Ivády, V.; Klimov, P. V.; Miao, K. C.; Falk, A. L.; Christle, D. J.; Szász, K.; Abrikosov, I. A.; Awschalom, D. D.; Gali, A. High-Fidelity Bidirectional Nuclear Qubit Initialization in SiC. *Phys. Rev. Lett.* **2016**, *117*, 220503.
(50) Isoya, J.; Retzker, A.; Plenio, M. B.; Schwartz, I.; Carl, P.; Jelezko, F.; Luy, B.; Scheuer, J.; Höfer, P.; Naydenov, B.; et al. Optically Induced Dynamic Nuclear Spin Polarisation in Diamond. *New J. Phys.* **2016**, *18*, No. 013040.
(51) Schwartz, I.; Scheuer, J.; Tratzmiller, B.; Müller, S.; Chen, Q.; Dhand, I.; Wang, Z.; Müller, C.; Naydenov, B.; Jelezko, F.; et al. Robust Optical Polarization of Nuclear Spin Baths Using Hamiltonian Engineering of Nitrogen-Vacancy Center Quantum Dynamics. *Sci. Adv.* **2018**, *4*, No. eaat8978.
(52) Chen, Q.; Schwarz, I.; Jelezko, F.; Retzker, A.; Plenio, M. B. Optical Hyperpolarization of ^{13}C Nuclear Spins in Nanodiamond Ensembles. *Phys. Rev. B: Condens. Matter Mater. Phys.* **2015**, *92*, 184420.
(53) Falk, A. L.; Klimov, P. V.; Buckley, B. B.; Ivády, V.; Abrikosov, I. A.; Calusine, G.; Koehl, W. F.; Gali, Á.; Awschalom, D. D. Electrically and Mechanically Tunable Electron Spins in Silicon Carbide Color Centers. *Phys. Rev. Lett.* **2014**, *112*, 187601.

https://dx.doi.org/10.1021/acs.jpclett.0c00052
J. Phys. Chem. Lett. 2020, 11, 1675−1681